

**Two-body photodisintegration of  ${}^4\text{He}$  with full final state interaction**

Sofia Quaglioni, Winfried Leidemann, and Giuseppina Orlandini

*Dipartimento di Fisica, Università di Trento, and Istituto Nazionale di Fisica Nucleare, Gruppo Collegato di Trento, I-38050 Povo, Italy*

Nir Barnea

*The Racah Institute of Physics, The Hebrew University, 91904 Jerusalem, Israel*

Victor D. Efros

*Russian Research Centre "Kurchatov Institute," Kurchatov Square, 1, 123182 Moscow, Russia*

(Received 19 November 2003; published 6 April 2004)

The cross sections of the processes  ${}^4\text{He}(\gamma,p){}^3\text{H}$  and  ${}^4\text{He}(\gamma,n){}^3\text{He}$  are calculated taking into account the full final state interaction via the Lorentz integral transform method. This is the first consistent microscopic calculation beyond the three-body breakup threshold. The results are obtained with a semirealistic central nucleon-nucleon potential including also the Coulomb force. The cross sections show a pronounced dipole peak at 27 MeV which lies within the rather broad experimental band. At higher energies, where experimental uncertainties are considerably smaller, one finds a good agreement between theory and experiment. The calculated sum of three- and four-body photodisintegration cross sections is also listed and is in fair agreement with the data.

DOI: 10.1103/PhysRevC.69.044002

PACS number(s): 25.20.Dc, 21.45.+v, 24.30.Cz, 27.10.+h

**I. INTRODUCTION**

The photodisintegration of the  ${}^4\text{He}$  nucleus has a long-standing history. First experiments on the  $(\gamma,n)$  reaction were performed some 50 years ago [1]. In the following 25 years various experimental groups carried out measurements for both the  ${}^4\text{He}(\gamma,p){}^3\text{H}$  and  ${}^4\text{He}(\gamma,n){}^3\text{He}$  reaction channels and the inverse capture reactions [2–15]. Dramatically conflicting results have been obtained as a result of this work. The  $(\gamma,p)$  data were consistent in showing a rather pronounced resonant peak close to the three-body breakup threshold. At the same time, the  $(\gamma,n)$  data at low energy were very spread, and measurements showed either a strongly pronounced or a rather suppressed giant dipole peak. In 1983 a careful and balanced review of all the available experimental data for the two mirror reactions was provided [16]. A strongly peaked cross section at low energy for the  $(\gamma,p)$  channel and a flatter shape for the  $(\gamma,n)$  one was recommended by the authors. Three new experiments on the  $(\gamma,p)$  reaction were subsequently carried out, two of them contradicting and one confirming the recommended cross section. In particular, in Refs. [17] and [18] a suppressed dipole resonance was found, whereas Ref. [19] proved to be in agreement with the previous strongly peaked results. Measurements of the ratio of the  $(\gamma,p)$  to  $(\gamma,n)$  cross sections in the giant resonance region were performed as well and, at variance with the cross sections recommended in Ref. [16], results very close to unity were reported [20,21]. Finally, in 1992 additional cross section data were deduced from a Compton scattering experiment on  ${}^4\text{He}$  [22]. A strongly peaked cross section for the  ${}^4\text{He}$  total photoabsorption was found suggesting a  $(\gamma,n)$  cross section considerably larger than the one recommended in Ref. [16].

In 1996 the first theoretical calculation of the two-fragment breakup cross section with inclusion of final state

interaction (FSI) was performed in the energy range below the three-fragment breakup threshold [23]. The semirealistic MTI-III potential [24] was employed. The results of Ref. [23] showed a rather suppressed giant dipole peak. In the following year a calculation of the total  ${}^4\text{He}$  photoabsorption cross section up to the pion threshold was carried out [25]. Full FSI was taken into account in the whole energy range via the Lorentz integral transform (LIT) method [26] that does not require calculating continuum wave functions. The four-nucleon dynamics was described with the same nucleon-nucleon ( $NN$ ) potential as in Ref. [23]. Different from the previous work a pronounced giant dipole peak was found. These results have been reexamined in Ref. [27]. A small shift of the peak position has been obtained, but the pronounced peak has been confirmed.

In order to understand the origin of the large total photo-nuclear cross section in terms of the various channel contributions, a separate calculation of the channel cross sections is necessary. The present paper reports a theoretical study of the two-fragment breakup processes  ${}^4\text{He}(\gamma,p){}^3\text{H}$  and  ${}^4\text{He}(\gamma,n){}^3\text{He}$ . For these exclusive reactions we investigate the issue of the giant dipole peak height, and we also calculate the cross section at higher energies, up to the pion threshold. The calculation includes full FSI via the LIT method [28] and employs the semirealistic MTI-III potential [24].

The LIT method has already been successfully tested for exclusive reactions in the  $d(e,e'p)n$  process [29]. The present calculation represents the first application to  $A > 2$ . We would like to emphasize that in our study FSI is taken into account rigorously also beyond the three- and four-body breakup thresholds. In addition, combining our cross sections with the total photoabsorption cross section calculated in Refs. [25,27] for the same potential, we obtain the sum of

three- and four-body photodisintegration cross sections of  ${}^4\text{He}$ , for which some experimental data are available [30–33].

## II. GENERAL FORMALISM

### A. Cross section

The total exclusive cross section of the  ${}^4\text{He}$  photodisintegration into the two fragments  $N$  and 3, where  $N$  refers to the scattered proton (neutron) and 3 refers to the  ${}^3\text{H}$  ( ${}^3\text{He}$ ) nucleus, is given by

$$\begin{aligned} \sigma_{N,3} &= 4\pi^2 \frac{e^2}{\hbar c} k\mu\omega_\gamma \\ &\times \sum_{M_3, M_N = \pm \frac{1}{2}} \int |\langle \Psi_{N,3}^-(E_{N,3}) | D_z | \Psi_\alpha \rangle|^2 d\Omega_k, \\ E_{N,3} &= \omega_\gamma + E_\alpha. \end{aligned} \quad (1)$$

In the equation above we neglect the very small nuclear recoil energy. With  $\mu$  and  $k$  we denote the reduced mass and the relative momentum of the fragments, respectively,  $\omega_\gamma$  is the incident photon energy,  $\Psi_\alpha$  is the ground-state wave function,  $\Psi_{N,3}^-$  is the final-state continuum wave function of the minus type pertaining to the  $N, 3$  channel [34], and  $E_\alpha$  and  $E_{N,3}$  are the energies of the corresponding initial and final states ( $E_{N,3} = k^2/2\mu + E_3$ ,  $E_3$  being the energy of fragment 3), respectively. The sum goes over projections  $M_3$  and  $M_N$  of the fragment angular momenta in the final state. The continuum states  $\Psi_{N,3}^-$  are normalized to  $\delta(\mathbf{k} - \mathbf{k}') \delta_{M_3 M_3'} \delta_{M_N M_N'}$ .

As in Refs. [25,27] only transitions induced by the unretarded dipole operator,

$$D_z = \sum_{j=1}^4 \frac{1 + \tau_j^3}{2} z_j, \quad (2)$$

are taken into account. Here  $\tau_j^3$  denotes the third component of the  $j$ th nucleon isospin and  $z_j$  represents the  $z$  component of the distance between the  $j$ th nucleon and the center of mass of the system. This form of the transition operator already includes the leading effects of meson exchange currents via Siegert's theorem. Additional contributions to the total cross section are small at the energies considered here (see also Refs. [35,36]).

The main difficulty in the calculation of such a cross section is the presence of the continuum wave function  $\Psi_{N,3}^-(E_{N,3})$  in the transition matrix element

$$T_{N,3}(E_{N,3}) = \langle \Psi_{N,3}^-(E_{N,3}) | D_z | \Psi_\alpha \rangle. \quad (3)$$

As will be explained in the following section, with the LIT method one is able to perform an *ab initio* calculation of this transition matrix element in the whole energy range below the pion threshold without dealing with the continuum solutions of the four-body Schrödinger equation.

### B. The LIT method for exclusive reactions

For the case of an exclusive perturbation-induced process, all the information about the reaction dynamics is contained in the transition matrix element of the perturbation  $\hat{O}$  between the initial ( $\Psi_0$ ) and final ( $\Psi_f^-$ ) states,

$$T_f(E_f) = \langle \Psi_f^-(E_f) | \hat{O} | \Psi_0 \rangle. \quad (4)$$

The calculation of such a matrix element can be carried out with the LIT method as outlined in the following [28,29]. For simplicity we restrict our discussion to an exclusive reaction leading to a final state with two fragments, a fragment  $a$  with  $n_a$  nucleons and a fragment  $b$  with  $n_b = A - n_a$  nucleons, though more complex fragmentations of the initial  $A$ -body system can be treated as well. Denoting with  $H$  the full nuclear Hamiltonian, we have a formal expression for  $\Psi_{f=a,b}^-$  in terms of the ‘‘channel state’’  $\phi_{f=a,b}^-(E_{f=a,b})$  [34],

$$|\Psi_{a,b}^-(E_{a,b})\rangle = \hat{A} |\phi_{a,b}^-(E_{a,b})\rangle + \frac{1}{E_{a,b} - i\epsilon - H} \hat{A} \mathcal{V} |\phi_{a,b}^-(E_{a,b})\rangle, \quad (5)$$

where  $\hat{A}$  is an antisymmetrization operator. In case that at least one of the fragments is chargeless, the channel state  $\phi_{a,b}^-(E_{a,b})$  is the product of the internal wave functions of the fragments and of their relative free motion. Correspondingly,  $\mathcal{V}$  in Eq. (5) is the sum of all interactions between particles belonging to different fragments. If both fragments are charged,  $\phi_{a,b}^-(E_{a,b})$  is chosen to account for the average Coulomb interaction between them, and the plane wave describing their relative motion is replaced by the Coulomb function of the minus type. Correspondingly,  $\mathcal{V}$  in Eq. (5) is the sum of all interactions between particles belonging to different fragments after subtraction of the average Coulomb interaction, already considered via the Coulomb function. We write  $\phi_{a,b}^-(E_{a,b})$  in the partial wave expansion form

$$\begin{aligned} \phi_{a,b}^-(E_{a,b}) &= \frac{\Phi_a(1, \dots, n_a) \Phi_b(n_a + 1, \dots, A)}{(2\pi)^{3/2}} \\ &\times 4\pi \sum_{\ell=0}^{\infty} \sum_{m=-\ell}^{\ell} i^\ell e^{-i\delta_\ell(k)} \frac{w_\ell(k; r)}{kr} Y_{\ell m}(\Omega_r) Y_{\ell m}^*(\Omega_k). \end{aligned} \quad (6)$$

Here  $\Phi_a(1, \dots, n_a)$  and  $\Phi_b(n_a + 1, \dots, A)$  are the internal wave functions of the fragments,  $\mathbf{r} = (r, \Omega_r) = \mathbf{R}_{\text{c.m.}}^a - \mathbf{R}_{\text{c.m.}}^b$  represents the distance between them, and the energy of the relative motion is  $k^2/2\mu = E_{a,b} - E_a - E_b$ , where  $E_a$  and  $E_b$  are the fragment ground-state energies. The functions  $w_\ell(k; r)$  are the regular Coulomb wave functions of order  $\ell$ , and  $\delta_\ell(k)$  are the Coulomb phase shifts [34].

The internal wave functions of the fragments are assumed to be antisymmetrized and normalized to unity, so that the properly normalized continuum wave function in Eq. (5) is obtained via application of the antisymmetrization operator

$$\hat{A} = \sqrt{\frac{n_a! n_b!}{A!}} \left[ 1 - \sum_{i=1}^{n_a} \sum_{j=n_a+i}^A \mathcal{P}_{ij} \right], \quad (7)$$

where  $\mathcal{P}_{ij}$  are particle permutation operators [34].

When one inserts Eq. (5) into Eq. (4) the transition matrix element becomes the sum of two pieces, a Born term,

$$T_{a,b}^{\text{Born}}(E_{a,b}) = \langle \phi_{a,b}^-(E_{a,b}) | \hat{A} \hat{O} | \Psi_0 \rangle, \quad (8)$$

and an FSI dependent term,

$$T_{a,b}^{\text{FSI}}(E_{a,b}) = \left\langle \phi_{a,b}^-(E_{a,b}) \left| \mathcal{V} \hat{A} \frac{1}{E_{a,b} + i\varepsilon - H} \hat{O} \right| \Psi_0 \right\rangle. \quad (9)$$

While the Born term is rather simple to deal with, the determination of the FSI dependent matrix element is rather complicated. We treat this term within the LIT approach as outlined in the following.

Let  $\Psi_\nu(E_\nu)$  be the eigenstates of the Hamiltonian labeled by channel quantum numbers  $\nu$  and normalized as  $\langle \Psi_\nu | \Psi_{\nu'} \rangle = \delta(\nu - \nu')$ . Using the completeness relation of the set  $\Psi_\nu(E_\nu)$ , the matrix element  $T_{a,b}^{\text{FSI}}(E_{a,b})$  can be written as

$$\begin{aligned} T_{a,b}^{\text{FSI}}(E_{a,b}) &= \int d\nu \langle \phi_{a,b}^-(E_{a,b}) | \mathcal{V} \hat{A} | \Psi_\nu(E_\nu) \rangle \\ &\quad \times \frac{1}{E_{a,b} + i\varepsilon - E_\nu} \langle \Psi_\nu(E_\nu) | \hat{O} | \Psi_0 \rangle \\ &= \int_{E_{th}^-}^{\infty} \frac{F_{a,b}(E)}{E_{a,b} + i\varepsilon - E} dE \\ &= -i\pi F_{a,b}(E_{a,b}) \\ &\quad + \mathcal{P} \int_{E_{th}^-}^{\infty} \frac{F_{a,b}(E)}{E_{a,b} - E} dE, \end{aligned} \quad (10)$$

where  $F_{a,b}(E)$  is defined as

$$\begin{aligned} F_{a,b}(E) &= \int d\nu \langle \phi_{a,b}^-(E_{a,b}) | \mathcal{V} \hat{A} | \Psi_\nu(E_\nu) \rangle \\ &\quad \times \langle \Psi_\nu(E_\nu) | \hat{O} | \Psi_0 \rangle \delta(E - E_\nu), \end{aligned} \quad (11)$$

and  $E_{th}$  is the lowest excitation energy in the system, i.e., the breakup threshold energy. To calculate  $T_{a,b}^{\text{FSI}}$  one needs to know the function  $F_{a,b}$  for all energy values. The direct calculation of  $F_{a,b}$  is of course far too difficult, since one should know all the eigenstates  $\Psi_\nu$  for the whole eigenvalue spectrum of  $H$ . However, an indirect calculation of  $F_{a,b}$  is possible applying the LIT method. To this end, one introduces an integral transform of  $F_{a,b}$  with a kernel of Lorentzian shape,

$$\begin{aligned} L[F_{a,b}](\sigma) &= \int_{E_{th}^-}^{\infty} \frac{F_{a,b}(E)}{(E - \sigma_R)^2 + \sigma_I^2} dE \\ &= \int_{E_{th}^-}^{\infty} \frac{F_{a,b}(E)}{(E - \sigma)(E - \sigma^*)} dE \\ &= \int d\nu \left\langle \phi_{a,b}^-(E_{a,b}) \left| \mathcal{V} \hat{A} \frac{1}{H - \sigma^*} \right| \Psi_\nu(E_\nu) \right\rangle \\ &\quad \times \left\langle \Psi_\nu(E_\nu) \left| \frac{1}{H - \sigma} \hat{O} \right| \Psi_0 \right\rangle \\ &= \langle \widetilde{\Psi}_2(\sigma) | \widetilde{\Psi}_1(\sigma) \rangle, \end{aligned} \quad (12)$$

with  $\sigma = \sigma_R + i\sigma_I$ . Here we denote

$$\widetilde{\Psi}_1(\sigma) = (H - \sigma)^{-1} \hat{O} | \Psi_0 \rangle,$$

$$\widetilde{\Psi}_2(\sigma) = (H - \sigma)^{-1} \hat{A} \mathcal{V} | \phi_{a,b}^-(E_{a,b}) \rangle. \quad (13)$$

Equation (12) shows that  $L[F_{a,b}](\sigma)$  can be calculated without explicit knowledge of  $F_{a,b}$  provided that one solves the two equations,

$$(H - \sigma) | \widetilde{\Psi}_1 \rangle = \hat{O} | \Psi_0 \rangle, \quad (14)$$

$$(H - \sigma) | \widetilde{\Psi}_2 \rangle = \hat{A} \mathcal{V} | \phi_{a,b}^-(E_{a,b}) \rangle, \quad (15)$$

which differ in the source terms only.

It can be seen that  $\widetilde{\Psi}_1$  and  $\widetilde{\Psi}_2$  are localized, i.e., have finite norms. Assuming that  $\sigma_I \neq 0$ , this is ensured by the fact that the source terms in the right-hand sides of Eqs. (14) and (15) are localized. In fact in the coordinate representation the source term in Eq. (14) decreases exponentially for increasing distances between particles. The source term in Eq. (15) contains two potential contributions, i.e., the nuclear force component and the Coulomb interaction. The contribution due to the nuclear interaction vanishes exponentially for increasing distances between particles. Since the average Coulomb potential between the fragments is already taken into account via Eq. (6), the remaining Coulomb contribution behaves like  $r^{-2}$ , as the distance  $r$  from the fragments increases. Therefore, the source term remains localized also in the presence of the Coulomb force. In our calculation this Coulomb term arises in case of the  $p$ ,  ${}^3\text{H}$  channel and its contribution to the results is found to be very small.

In case of breakups into more than two fragments it is convenient to write Eq. (12) in another form:

$$\begin{aligned} L[F_{a,b}](\sigma) &= \frac{1}{2i\sigma_I} \left\langle \phi^-(E_{a,b}) \left| \mathcal{V} \hat{A} \left[ \frac{1}{H - \sigma} - \frac{1}{H - \sigma^*} \right] \hat{O} \right| \Psi_0 \right\rangle \\ &= \frac{1}{2i\sigma_I} [\langle \phi_{a,b}^-(E_{a,b}) | \mathcal{V} \hat{A} | \widetilde{\Psi}_1(\sigma) \rangle \\ &\quad - \langle \phi_{a,b}^-(E_{a,b}) | \mathcal{V} \hat{A} | \widetilde{\Psi}_1'(\sigma) \rangle]. \end{aligned} \quad (16)$$

Here  $\widetilde{\Psi}_1(\sigma)$  is the same as above, and  $\widetilde{\Psi}_1'(\sigma)$  satisfies

$$(H - \sigma^*)|\widehat{\Psi}'_1(\sigma)\rangle = \hat{O}|\Psi_0\rangle. \quad (17)$$

Therefore, also in this case, one has to deal with a localized solution.

When solving Eqs. (14), (15), and (17), it is sufficient to require that the solutions are localized, and no other boundary conditions are to be imposed. Therefore, similar to what is done in bound-state calculations, one can use an expansion over a basis set of localized functions. A convenient choice is the basis set consisting of correlated hyperspherical harmonics (CHH) multiplied by hyperradial functions.

As discussed in Ref. [27] for the case of the total  ${}^4\text{He}$  photoabsorption cross section, special attention has to be paid to the convergence of such expansions. A rather large number of basis states is necessary in order to reach convergence, thus leading to large Hamiltonian matrices. Instead of using a time consuming inversion method we directly evaluate the scalar products in Eq. (16) with the Lanczos technique [37]. Inserting the Lanczos orthonormal basis  $\{\varphi_i, i=0, \dots, n\}$  into Eq. (16), where  $\varphi_o$  is taken to be the right-hand side (normalized to unity) of Eqs. (14) and (17), one gets

$$L[F_{a,b}](\sigma) = \frac{\sqrt{\langle\Psi_0|\hat{O}^\dagger\hat{O}|\Psi_0\rangle}}{2i\sigma_I} \sum_{i=0}^n \langle\phi_{a,b}^-(E_{a,b})|\mathcal{V}\hat{A}|\varphi_i\rangle \times \left\langle \varphi_i \left| \frac{1}{H-\sigma} - \frac{1}{H-\sigma^*} \right| \varphi_o \right\rangle. \quad (18)$$

The matrix elements  $\langle\varphi_i|(H-\sigma)^{-1}|\varphi_o\rangle$  can be written as continued fractions of the Lanczos coefficients.

After having calculated  $L[F_{a,b}](\sigma)$  one obtains the function  $F_{a,b}(E)$ , and thus  $T_{a,b}(E_{a,b})$ , via the inversion of the LIT, as described in Ref. [38].

### III. RESULTS

The ground states of  ${}^4\text{He}$ ,  ${}^3\text{He}$ , and  ${}^3\text{H}$  as well as the LIT in Eq. (18) are calculated using the CHH expansion method. In order to speed up the convergence, state independent correlations are introduced as in Ref. [39]. We use the MTI-III [24] potential and identical CHH expansions for the ground-state wave functions of  ${}^4\text{He}$  and of the three-nucleon systems as in Refs. [27,40], respectively.

Because of the choice of the excitation operator [see Eq. (2)], in solving Eqs. (14) and (15) the hyperspherical harmonics (HH) must be characterized by the quantum numbers  $L=1$ ,  $S=0$ , and  $T=1$ . In this calculation the maximal value of the grand-angular quantum number  $K_{max}$  is equal to 29. Such a high value of  $K_{max}$  has been made possible by neglecting states which have proved to give very small contributions to the LIT. The selection of states has been done in the following way. Our HH depend on three Jacobi vectors  $\xi_1, \xi_2, \xi_3$ , among which  $\xi_1$  represents the distance between a pair of particles. The HH entering the calculation are obtained via symmetrization of the HH possessing a definite relative orbital momentum  $\ell_1$  associated with  $\xi_1$  and a definite grand-angular momentum  $\widetilde{K}$  in the subspace of vectors  $\xi_2, \xi_3$ . We have found that beyond  $K_{max}=13$  we can neglect all symme-

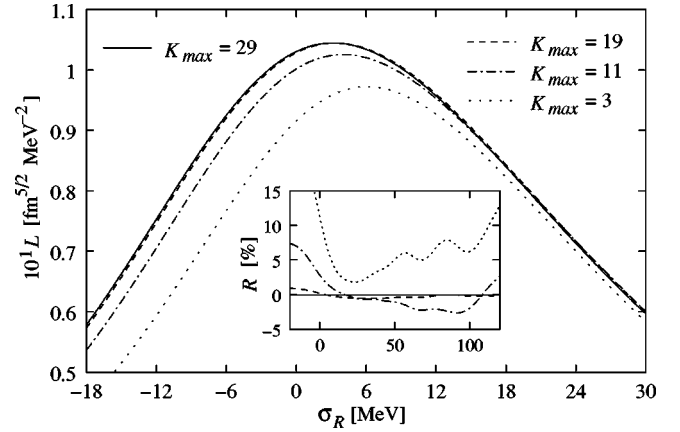


FIG. 1. The Lorentz transform of Eq. (18) for  $\sigma_\gamma=20$  MeV at  $E_{n,{}^3\text{He}}=27.9$  MeV with various  $K_{max}$  values. In the inset the deviations  $R=100[L(K_{max}=29)-L(K_{max})]/L(K_{max}=29)$  are shown.

trized HH which originate from the nonsymmetrized HH with  $\ell_1$  greater than 2 and  $\widetilde{K}$  greater than 3 and, beyond  $K_{max}=19$ , those with  $\ell_1$  greater than 0 and  $\widetilde{K}$  greater than 1. This selection is similar to that justified and used in noncorrelated HH bound-state calculations (see Ref. [41] and references therein). An additional selection has been performed with respect to the permutational symmetry types of the HH. For the quantum numbers  $S=0$ ,  $T=1$ , HH of two permutational symmetry types enter the expansion, those belonging to the irreducible representations  $[f]=[+]$  and  $[f]=[-]$  of the four-particle permutation group  $S_4$  [39,41]. For basis states constructed from the HH of the  $[+]$  type the probability for a nucleon pair to be in a relative even state and, in particular, in the  $s$  state is substantially higher. We have found that the contribution to the LIT of states with the spatial symmetry  $[-]$  is suppressed, and the corresponding HH with  $K$  values higher than 9 can be neglected in the calculation.

In Fig. 1, the convergence of the LIT with respect to  $K_{max}$  is shown. One sees that for  $K_{max}=29$  a good convergence is reached.

In Fig. 2 we present our results for the  ${}^4\text{He}(\gamma, n){}^3\text{He}$  cross section together with experimental data. The shaded area around the full result represents an estimate of the uncertainties of our calculation, which will be explained below, in connection with the comparison of the present result with that obtained in the inclusive case. The difference between the total cross section and its Born approximation shows large effects of FSI. At small energies FSI enhances the transition matrix element since the final-state continuum wave function inside the reaction zone becomes larger due to the attraction between the fragments. At higher energies the transition matrix element including FSI becomes smaller than the Born one. This is due to shorter wavelengths (higher particle momenta) leading to faster oscillations in the integrands.

As it was pointed out in the Introduction, the experimental results do not show a unique picture. In the energy region beyond 35 MeV there is an overall agreement of the data of Refs. [4,6,8,9,11,12,42], whereas in the dipole resonance region big discrepancies are present. The data from Refs.

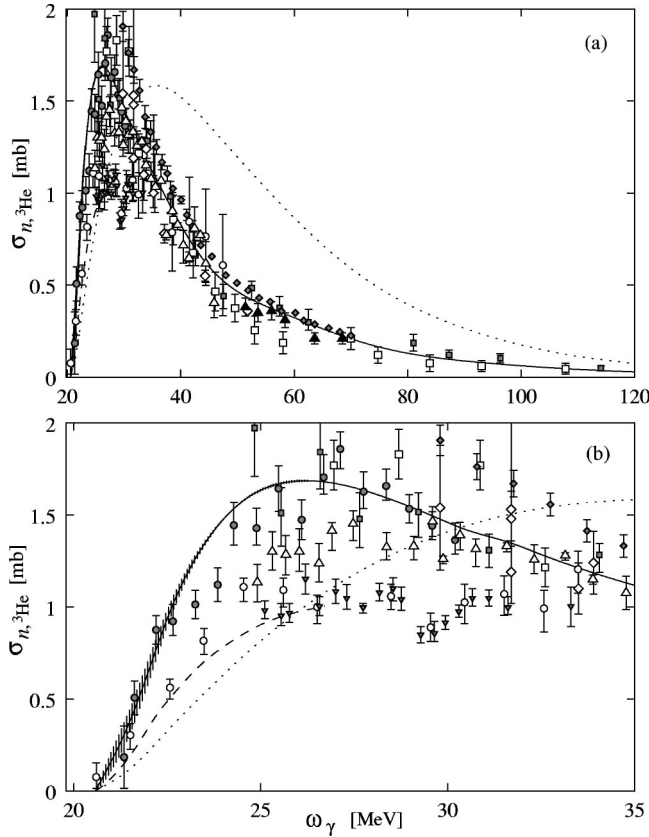


FIG. 2.  ${}^4\text{He}(\gamma, n){}^3\text{He}$  cross section up to 120 MeV (a) and 35 MeV (b): full result with FSI included (solid curve), Born approximation only (dotted curve), full result from Ref. [23] (dashed curve). The shaded area around the full line represents the uncertainties of our calculation (see text). Experimental data up to 1983: Ref. [4] (full gray squares), Ref. [6] (open diamonds), Ref. [8] (full gray diamonds), Ref. [9] (open squares), Ref. [10] (full gray circles), Ref. [11] (open upward triangles), Ref. [12] (open circles), Ref. [13] (full gray downward triangles). Experimental data after 1983: Ref. [42] (full black upward triangles).

[4,8–10] show a rather pronounced dipole peak, while the more recent ones from Refs. [12,13] show a flatter behavior [for more detailed information see also reviews of  $(\gamma, n)$  experiments [12,16]]. In the low-energy region our full calculation favors the strongly peaked data of Refs. [4,8–10]. It is seen from the figure that the higher-energy experimental cross section agrees quite well with our full calculation. We would like to point out the large effect of FSI in the high-energy tail. This is probably the region where large dependences of the cross sections from the details of the force and in particular of the three-body force are expected (see Ref. [43]) and where it would be desirable to have more accurate data.

In Fig. 2 also the  ${}^4\text{He}(\gamma, n){}^3\text{He}$  cross section of Ellerkmann *et al.* [23], obtained with the MTI-III potential, is shown. It is evident that the two theoretical results are at variance. In Ref. [23] the cross section is calculated using Alt-Grassenberger-Sandhas- (AGS)-type integral equations. Since the Born matrix element [see Eq. (8)] is an ingredient of both the AGS calculation and ours, it is instructive to make a comparison between the two cross sections in Born

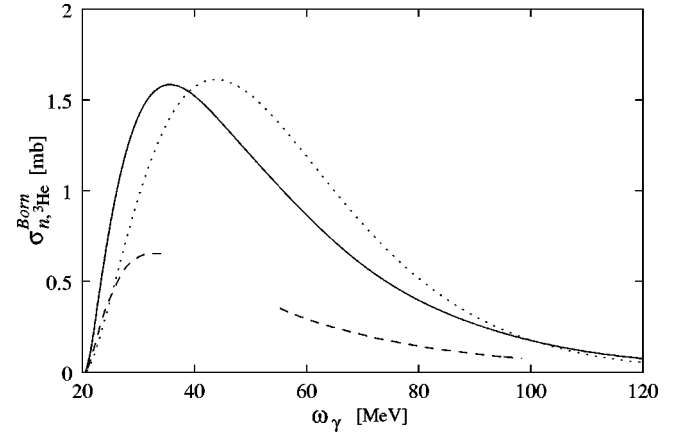


FIG. 3.  ${}^4\text{He}(\gamma, n){}^3\text{He}$  in Born approximation: CHH (solid curve), available results from Ref. [23] (dashed curve), BMCS (dotted curve).

approximation, since in this case only the ground-state wave functions of  ${}^3\text{He}$  and  ${}^4\text{He}$  are needed. In Fig. 3 the Born cross sections are shown. The result of Ref. [23] has a very similar shape as ours, but a much reduced strength (about 60 %).

In Ref. [23] the  ${}^3\text{He}$  and  ${}^4\text{He}$  bound states are determined by solving the homogeneous three- and four-nucleon AGS equations via the  $W$ -matrix method [44] and the energy-dependent pole expansion (EDPE) [45]. As already stated above, our  ${}^3\text{He}$  and  ${}^4\text{He}$  bound states are calculated using the CHH expansion as in Refs. [27] and [40]. As a simple test we perform an analytical calculation using simple  $A$ -body bound-state wave functions ( $A=3, 4$ ) of the type

$$\Psi_A = \left( \frac{2b_A}{\pi} \right)^{3(A-1)/4} \prod_{i=1}^A e^{-b_A |\mathbf{r}_i - \mathbf{R}_{\text{c.m.}}^{(A)}|^2} \chi_{T_A S_A}^a, \quad (19)$$

where  $\chi_{T_A S_A}^a$  represents the antisymmetric spin-isospin function and  $b_A$  is a free parameter.

This leads to the following Born model cross section (BMCS):

$$\sigma_{n, {}^3\text{He}}^{\text{Born}} = 4\pi^2 \frac{e^2}{\hbar c} k \mu \omega_\gamma \left( \frac{4}{3} \right)^{9/2} \frac{4 b_3^3}{\sqrt{2\pi b_4 (b_3 + b_4)^6}} k^2 e^{-2k^2/3b_4}. \quad (20)$$

If we choose the parameters  $b_3=0.167 \text{ fm}^{-2}$  and  $b_4=0.279 \text{ fm}^{-2}$  in order to reproduce the same rms radii of  ${}^3\text{He}$  (1.73 fm) and  ${}^4\text{He}$  (1.42 fm) as for the MTI-III potential we obtain the BMCS result shown in Fig. 3. The BMCS and Born CHH results have almost identical peak heights, while the peak positions are shifted by about 10 MeV.

We have calculated the BMCS result both by using directly the analytical expression of Eq. (20) and by our computer code, and found identical results.

The  ${}^4\text{He}(\gamma, p){}^3\text{H}$  cross section is compared with data in Fig. 4. The experimental situation is similar to the  $(\gamma, n)$  case considered above. Again some experimental results show a

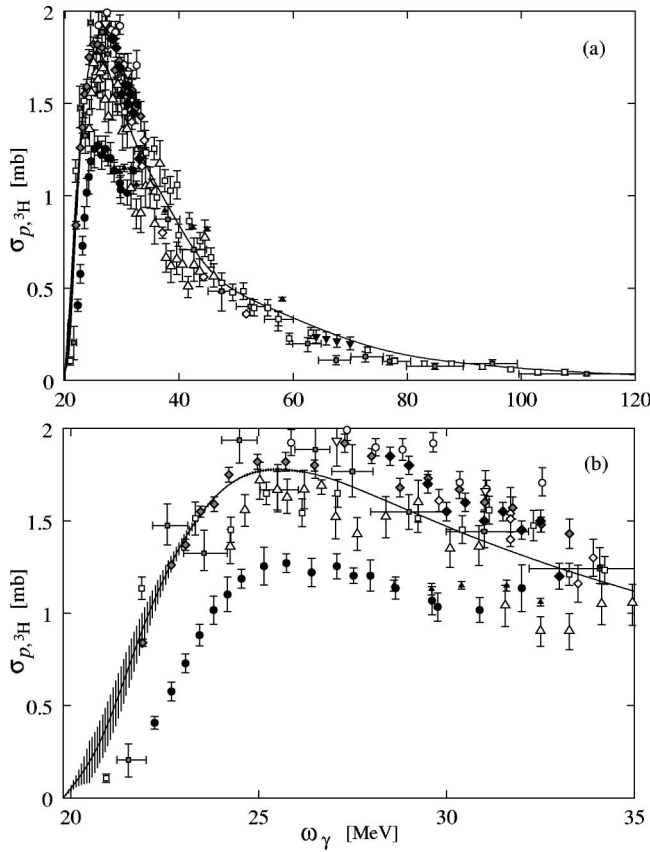


FIG. 4.  ${}^4\text{He}(\gamma,p){}^3\text{H}$  cross section up to 120 MeV (a) and 35 MeV (b): full result with FSI included (solid curve); experimental data up to 1983 from Ref. [4] (full gray squares), Ref. [5] (full gray diamonds), Ref. [6] (open diamonds), Ref. [9] (open squares), Ref. [11] (open upward triangles), Ref. [14] (open circles), Ref. [15] (open downward triangles); experimental data after 1983 from Ref. [17] (full black upward triangles), Ref. [18] (full black circles), Ref. [19] (full black diamonds), and Ref. [46] (full black downward triangles).

pronounced giant dipole peak at low energies, as in case of Refs. [4–6,9,11,14,15], and others present much less strength, such as Refs. [17] and [18]. At higher energies there is quite a satisfactory agreement among experimental data of different groups. As in the  ${}^4\text{He}(\gamma,n){}^3\text{He}$  case, our full results have a large cross section in the dipole resonance region and favor the strongly peaked data, while beyond the peak one finds a rather good agreement between our calculation and all data.

In Fig. 5 we show the effect of the Coulomb interaction in the  ${}^4\text{He}(\gamma,N){}^3$  reactions. As expected, it is very small all over the energy range.

Since the  ${}^4\text{He}(\gamma,d)d$  reaction is not induced by the dipole operator of Eq. (2), the sum of the  ${}^4\text{He}(\gamma,p){}^3\text{H}$  and  ${}^4\text{He}(\gamma,n){}^3\text{He}$  cross sections has to be equal to the  ${}^4\text{He}$  total inclusive photoabsorption cross section below the  $n+p+d$  breakup threshold. Comparison of the sum of our exclusive cross sections in this region with the total inclusive photoabsorption cross section calculated independently can therefore serve as a test of our results. To this aim, we have calculated also the total photoabsorption cross section. This was done

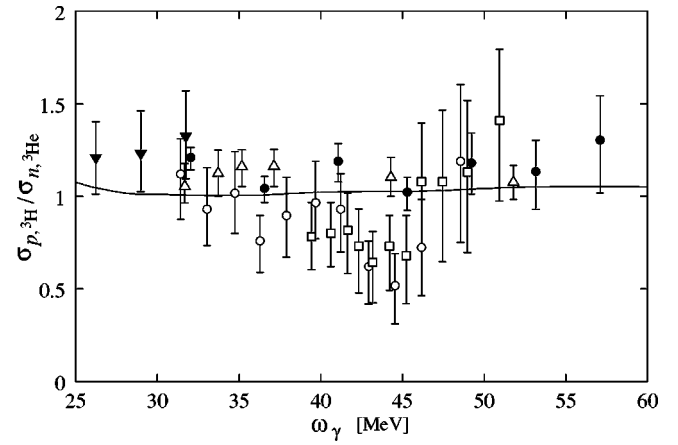


FIG. 5. Ratio between the  ${}^4\text{He}(\gamma,p){}^3\text{H}$  and the  ${}^4\text{He}(\gamma,n){}^3\text{He}$  cross sections (solid curve); experimental data up to 1983 from Ref. [20] (open circles and open squares), Ref. [6] (reanalyzed, as reported in Ref. [20]) (open upward triangles); experimental data after 1983 from Ref. [21] (full black circles and full black downward triangles).

using the fact that the norm  $\langle \widehat{\Psi}_1(\sigma) | \widehat{\Psi}_1(\sigma) \rangle$  represents the LIT of this total cross section. Our present CHH calculation reproduces the results obtained for the total photoabsorption cross section with the effective interaction HH method [27]. This can be considered as one more test of our calculation, and this is accomplished thanks to the present efforts made in order to increase the  $K_{max}$  value up to 29.

The comparison of the sum of our cross sections for the  ${}^4\text{He}(\gamma,p){}^3\text{H}$  and  ${}^4\text{He}(\gamma,n){}^3\text{He}$  reactions with the CHH total photoabsorption cross section below the three-body breakup threshold is presented in Fig. 6. The agreement of the two curves in this region is quite satisfactory. There is only some discrepancy very close to threshold. The discrepancy could presumably be resolved by a calculation of the LIT in the threshold region with a smaller  $\sigma_f$ . However, this also requires an increase of the number of hyperradial basis functions along with a more precise determination of the nine-

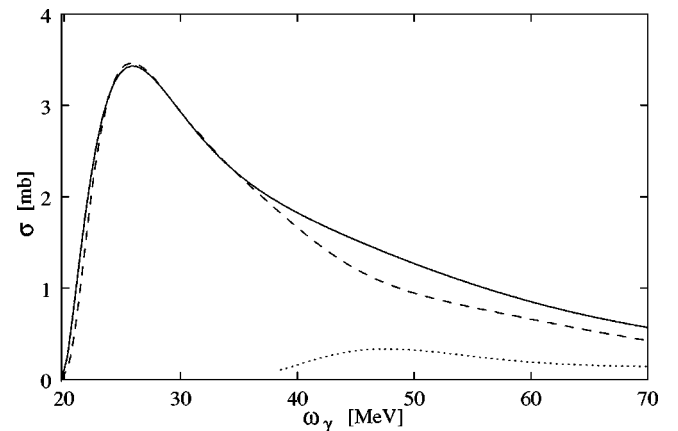


FIG. 6. Total  ${}^4\text{He}$  photoabsorption cross section (solid curve) compared to the sum of  ${}^4\text{He}(\gamma,p){}^3\text{H}$  and  ${}^4\text{He}(\gamma,n){}^3\text{He}$  cross sections (dashed curve); more-body breakup cross section obtained by subtraction (dotted curve).

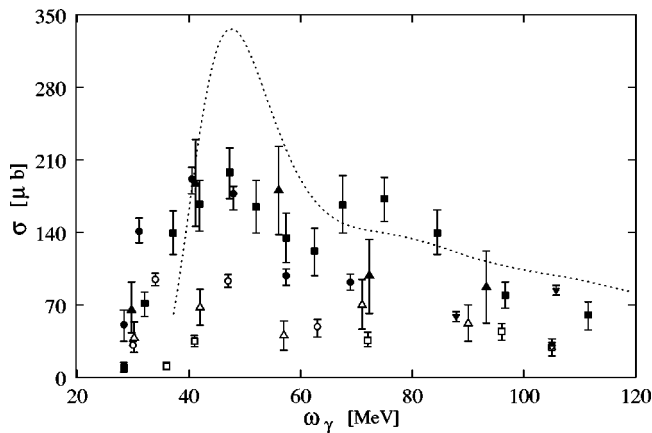


FIG. 7. More-body breakup cross section (same dotted curve as in Fig. 6).  ${}^4\text{He}(\gamma, pn)d$  (full symbols) and  ${}^4\text{He}(\gamma, 2p2n)$  (open symbols): experimental data up to 1983 from Ref. [30] (upward triangles), Ref. [31] (squares), Ref. [32] (circles); experimental data after 1983 from Ref. [33] (downward triangles).

dimensional integrals (at present Monte Carlo integrations), and thus a considerable improvement of the numerical calculation. At present this discrepancy has to be considered as an estimate of the uncertainty of our result. This uncertainty is in any case smaller than the error bars of available experiments in that energy range.

Figure 6 also shows an indirect determination of the three- and four-body breakup cross sections, which is obtained by subtraction of the  ${}^4\text{He}(\gamma, p){}^3\text{H}$  and  ${}^4\text{He}(\gamma, n){}^3\text{He}$  cross sections from the total photoabsorption cross section in the region where significant differences are found. This more-body breakup cross section is shown in Fig. 7 together with the three- and four-body disintegration data. Though there are some differences at lower energies and the peak of the theoretical cross section is more pronounced, one finds an overall fair agreement between theory and experiment.

In conclusion we summarize our work. We have calculated the total photodisintegration cross section of  ${}^4\text{He}$  in the

two mirror channels  $p, {}^3\text{H}$  and  $n, {}^3\text{He}$  with the MTI-III potential using the LIT method and the CHH expansion. For the first time a microscopic calculation for these reactions has been carried out taking fully into account final state interaction also beyond the three- and four-body breakup thresholds. The pronounced dipole resonance found in the total photonuclear cross sections [25,27] is almost exhausted by the two-body break up channel. The  ${}^4\text{He}(\gamma, p){}^3\text{H}$  and  ${}^4\text{He}(\gamma, n){}^3\text{He}$  cross sections we obtain have a very similar structure. Both show a pronounced giant dipole resonance peak at low energy as obtained in a previous calculation of the total  ${}^4\text{He}$  photoabsorption cross section with the same  $NN$  potential model. This low-energy behavior of the cross section is in agreement with the experimental data of Refs. [4,5,8–10,14,15,19] whereas other measurements [12,13,17,18] show less strength. At higher energies there are much less differences among the experimental data and one finds a rather good agreement with the theoretical results. Our indirect determination of the sum of three- and four-body breakup cross sections shows an overall fair agreement with the sum of three- and four-body breakup data.

We hope to have convinced the reader that further theoretical and experimental efforts are necessary for a better understanding of the  ${}^4\text{He}$  photodisintegration. The present theoretical results are fully consistent and complete regarding the treatment of the dynamics in the initial and final state, though obtained with a simple  $NN$  potential. In order to confirm the size of the giant dipole peak one would need a more realistic description of this process considering modern realistic  $NN$  potentials together with a three-nucleon force.

#### ACKNOWLEDGMENTS

We would like to thank M. A. Marchisio for supplying us with the computer code for the Lanczos algorithm. S.Q. acknowledges ECT\* for support. The work of N.B. was supported by the Israel Science Foundation (Grant No. 202/02). V.D.E. thanks the Department of Physics of the University of Trento for support and hospitality.

- 
- [1] G. A. Fergusson, J. Halpern, R. Nathans, and P. F. Yergin, *Phys. Rev.* **95**, 776 (1954).
  - [2] H. G. Clerk, R. J. Stewart, and R. C. Morrison, *Phys. Lett.* **18**, 316 (1965).
  - [3] V. P. Denisov and L. A. Kul'chitskii, *Yad. Fiz.* **6**, 437 (1967) [*Sov. J. Nucl. Phys.* **6**, 318 (1968)].
  - [4] A. N. Gorbunov, *Phys. Lett.* **27B**, 436 (1968).
  - [5] W. E. Meyerhof, M. Suffert, and W. Feldman, *Numer. Algorithms* **A148**, 211 (1970).
  - [6] W. R. Dodge and J. J. Murphy, *Phys. Rev. Lett.* **28**, 839 (1972).
  - [7] J. D. Irish, R. G. Johnson, B. L. Berman, B. J. Thomas, K. G. McNeill, and J. W. Jury, *Phys. Rev. C* **8**, 1211 (1973).
  - [8] C. K. Malcom, D. V. Webb, Y. M. Shin, and D. M. Skopik, *Phys. Lett.* **47B**, 433 (1973).
  - [9] Yu. M. Arkatov, P. I. Vatsset, V. I. Voloshchuk, V. A. Zolenko, I. M. Prokhorets, and V. I. Chmil', *Yad. Fiz.* **19**, 1172 (1974) [*Sov. J. Nucl. Phys.* **19**, 598 (1974)].
  - [10] J. D. Irish, R. G. Johnson, B. L. Berman, B. J. Thomas, K. G. McNeill, and J. W. Jury, *Can. J. Phys.* **53**, 802 (1975).
  - [11] F. Balestra, E. Bollini, L. Busso, R. Garfagnini, C. Guaraldo, G. Piragino, R. Scrimaglio, and A. Zanini, *Nuovo Cimento Soc. Ital. Fis., A* **38A**, 145 (1977).
  - [12] B. L. Berman, D. D. Faul, P. Meyer, and D. L. Olson, *Phys. Rev. C* **22**, 2273 (1980).
  - [13] L. Ward, D. R. Tilley, D. M. Skopik, N. R. Roberson, and H. R. Weller, *Phys. Rev. C* **24**, 317 (1981).
  - [14] R. C. McBroom, H. R. Weller, N. R. Roberson, and D. R. Tilley, *Phys. Rev. C* **25**, 1644 (1982).
  - [15] J. R. Calarco, S. S. Hanna, C. C. Chang, E. M. Diener, E. Kuhlmann, and G. A. Fisher, *Phys. Rev. C* **28**, 483 (1983).

- [16] J. R. Calarco, B. L. Berman, and T. W. Donnelly, *Phys. Rev. C* **27**, 1866 (1983).
- [17] R. Bernabei, A. Chisholm, S. d'Angelo, M. P. De Pascale, P. Picozza, C. Schaerf, P. Belli, L. Casano, A. Incicchitti, D. Prosperi, and B. Girolami, *Phys. Rev. C* **38**, 1990 (1988).
- [18] G. Feldman, M. J. Balbes, L. H. Kramer, J. Z. Williams, H. R. Weller, and D. R. Tilley, *Phys. Rev. C* **42**, 1167 (1990).
- [19] L. Van Hoorebeke, R. Van de Vyver, V. Fiermans, D. Ryckbosch, C. Van den Abeele, and J. Dias, *Phys. Rev. C* **48**, 2510 (1993).
- [20] T. W. Phillips, B. L. Berman, D. D. Faul, J. R. Calarco, and J. R. Hall, *Phys. Rev. C* **19**, 2091 (1979).
- [21] R. E. J. Florizone, J. Asai, G. Feldman, E. L. Hallin, D. M. Skopik, J. M. Vogt, R. C. Haight, and S. M. Sterbenz, *Phys. Rev. Lett.* **72**, 3476 (1994).
- [22] D. P. Wells, D. S. Dale, R. A. Eisenstein, F. J. Federspiel, M. A. Lucas, K. E. Mellendorf, A. M. Nathan, and A. E. O'Neill, *Phys. Rev. C* **46**, 449 (1992).
- [23] G. Ellerkmann, W. Sandhas, S. A. Sofianos, and H. Fiedeldey, *Phys. Rev. C* **53**, 2638 (1996).
- [24] R. A. Malfliet and J. Tjon, *Nucl. Phys.* **A127**, 161 (1969).
- [25] V. D. Efros, W. Leidemann, and G. Orlandini, *Phys. Rev. Lett.* **78**, 4015 (1997).
- [26] V. D. Efros, W. Leidemann, and G. Orlandini, *Phys. Lett. B* **338**, 130 (1994).
- [27] N. Barnea, V. D. Efros, W. Leidemann, and G. Orlandini, *Phys. Rev. C* **63**, 057002 (2001).
- [28] V. D. Efros, *Yad. Fiz.* **41**, 1498 (1985) [*Sov. J. Nucl. Phys.* **41**, 949 (1985)]; *Yad. Fiz.* **62**, 1975 (1999) [*Phys. At. Nucl.* **62**, 1833 (1999)].
- [29] A. La Piana and W. Leidemann, *Nucl. Phys.* **A677**, 423 (2000).
- [30] A. N. Gorbunov and V. M. Spiridonov, *Zh. Eksp. Teor. Fiz.* **34**, 866 (1958) [*Sov. Phys. JETP* **34**, 600 (1958)]; A. N. Gorbunov, *Yad. Fiz.* **10**, 469 (1969) [*Sov. J. Nucl. Phys.* **10**, 268 (1969)].
- [31] Yu. M. Arkatov, A. V. Bazaeva, P. I. Vatsset, P. I. Voloshchuk, A. P. Klyucharev, and A. F. Khodyachikh, *Yad. Fiz.* **10**, 1123 (1969) [*Sov. J. Nucl. Phys.* **10**, 639 (1970)].
- [32] F. Balestra, L. Busso, R. Garfagnini, G. Piragino, and A. Zanini, *Nuovo Cimento Soc. Ital. Fis., A* **49**, 575 (1979).
- [33] S. M. Doran *et al.*, *Nucl. Phys.* **A559**, 347 (1993).
- [34] M. L. Goldberger and K. W. Watson, *Collision Theory* (Wiley, New York, 1964).
- [35] H. Arenhövel and M. Sanzone, *Few-Body Syst., Suppl.* **3**, 1 (1991).
- [36] J. Golak, R. Skibinski, W. Glöckle, H. Kamada, A. Nogga, H. Witala, V. D. Efros, W. Leidemann, G. Orlandini, and E. L. Tomusiak, *Nucl. Phys.* **A707**, 365 (2002).
- [37] M. A. Marchisio, N. Barnea, W. Leidemann, and G. Orlandini, *Few-Body Syst.* **33**, 259 (2003).
- [38] V. D. Efros, W. Leidemann, and G. Orlandini, *Few-Body Syst.* **26**, 251 (1999).
- [39] V. D. Efros, W. Leidemann, and G. Orlandini, *Phys. Rev. Lett.* **78**, 432 (1997).
- [40] V. D. Efros, W. Leidemann, and G. Orlandini, *Phys. Lett. B* **408**, 1 (1997).
- [41] B. A. Fomin and V. D. Efros, *Yad. Fiz.* **34**, 587 (1981) [*Sov. J. Nucl. Phys.* **34**, 327 (1981)].
- [42] D. A. Sims *et al.*, *Phys. Lett. B* **442**, 43 (1998).
- [43] V. D. Efros, W. Leidemann, G. Orlandini, and E. L. Tomusiak, *Phys. Lett. B* **484**, 223 (1997).
- [44] E. A. Bartnik, H. Haberzettl, and W. Sandhas, *Phys. Rev. C* **34**, 1520 (1986).
- [45] S. A. Sofianos, N. J. McGurk, and H. Fiedeldey, *Nucl. Phys.* **A318**, 285 (1979).
- [46] R. T. Jones, D. A. Jenkins, P. T. Debevec, P. D. Harty, and J. E. Knott, *Phys. Rev. C* **43**, 2052 (1991).